IEEE Access
Multidisciplinary | Rapid Review | Open Access Journal

Received May 17, 2019, accepted June 22, 2019, date of publication June 26, 2019, date of current version July 15, 2019.

Digital Object Identifier 10.1109/ACCESS.2019.2925108

Internal Overvoltage Identification of Distribution Network via Time-Frequency Atomic Decomposition

WEI GAO[1,2], RONG-JONG WAI[2], (Senior Member, IEEE), YU-FEI LIAO[3], MOU-FA GUO[1], AND YAN YANG[2]

[1]College of Electrical Engineering and Automation, Fuzhou University, Fuzhou 350108, China
[2]Department of Electronic and Computer Engineering, National Taiwan University of Science and Technology, Taipei 106, Taiwan
[3]Fuzhou Power Supply Company of State Grid Fujian Electric Power Company, Fuzhou 350009, China

Corresponding author: Rong-Jong Wai (rjwai@mail.ntust.edu.tw)

This work was financially supported in part by the Ministry of Science and Technology of Taiwan under Grant MOST 108-2221-E-011-080-MY3, and in part by the National Natural Science Foundation of China under Grant 51677030.

ABSTRACT Internal overvoltage accidents in the distribution network are likely to cause an equipment insulation breakdown and result in system power outages and economic losses. Therefore, an internal overvoltage identification method based on the time-frequency atomic decomposition is investigated in this study. Firstly, the overvoltage waveforms are divided into four time periods. Then, the waveforms during these four time periods are decomposed by the atomic decomposition algorithm to obtain the effective atoms from the waveforms. Moreover, the root-mean-square (RMS) value of the zero-sequence voltage, the dominant atom frequency, the total relative matching degree, and the effective atom frequency are extracted as major features. In addition, the layered identification of the overvoltage types can be realized by combining the corresponding identification criteria. The salient advantage is the features with low dimension and a high degree of discrimination. Various overvoltage types can be identified just by the corresponding thresholds, and it is easier to deploy in the field than conventional methods based on classifier training. The effectiveness of the proposed method is verified by experimental results, and it concludes that the proposed algorithm has high accuracy and strong adaptability.

INDEX TERMS Distribution network, internal overvoltage, atomic decomposition, effective atoms, hierarchical identification.

I. INTRODUCTION

An overvoltage situation generated by the change of system parameters due to the operation of the circuit breaker or the system failure is called an internal overvoltage in the power system. Because the reasons for the change of system parameters are various, the amplitude, oscillation frequency, and time duration of internal overvoltages are different. The internal overvoltage is usually divided into the operating overvoltage and the temporary overvoltage according to the main cause. The operating overvoltage mainly caused by the line switching, the capacitor switching and the intermittent arc grounding occurs in the electromagnetic transient transition process, and it has a short duration. The temporary overvoltage includes the ferroresonance overvoltage and the power-frequency voltage rising. It may even exist for a long time, and is called the steady-state overvoltage [1].

A distribution network has characteristics with a complex structure, multiple types of equipment and a low-insulation level. Therefore, 70% of overvoltage accidents in a whole power system occur in distribution networks [1], [2]. The defective equipment may cause insulation breakdown under the occurrence of overvoltage, and even cause explosion accidents, which may result in huge economic losses and personal hazards [2]. If the overvoltage type can be accurately and timely distinguished in the initial stage of internal overvoltage, it is helpful to find out the reason of the accident and evaluate the insulation state of the equipment. It can improve the self-healing capacity of the distribution network, ensure reliable power supply, and stabilize the power supply voltage.

The associate editor coordinating the review of this manuscript and approving it for publication was M. Jaya Bharata Reddy.

There are many overvoltage types, and some of them have high similarity in waveforms, which are easy to cause misjudgment. At present, the identification of overvoltage can be generally divided into two stages including feature extraction and classifier training. Effective features and appropriate classifiers are important for the identification of overvoltage. The feature extraction involves two steps including signal decomposition and feature construction. Since most of overvoltage signals are non-stationary, it is necessary to use time-frequency analysis to decompose them and obtain information in both time domain and frequency domain in order to construct distinguishing features. Until now, traditional methods via time-frequency analyses used in the overvoltage identification contain Wavelet transform [3]–[6], S-transform [7], and Hilbert-Huang transform [8], etc. Angrisani *et al.* [4] used discrete wavelet transform as a time-frequency analysis tool to obtain time-frequency characteristics of waveforms in different frequency bands. Mokryani *et al.* [5] evaluated the characteristic expression ability of various Daubechies series wavelet in overvoltage fault identification. In order to identify the overvoltage situation, Wang *et al.* [7] adopted S-transformation to extract overvoltage characteristics and construct six different features, which are input into fuzzy expert systems and support vector machine (SVM) to identify eight types of overvoltage. Babu and Mohan [8] decomposed voltage waveforms into a series of intrinsic mode function (IMF) components by the empirical mode decomposition (EMD), and then constructed the energy distribution of instantaneous amplitude, which was used to identify power system faults including short circuit and overvoltage. In general, these methods have a good effect in signal decomposition, but there are some shortcomings for different types of overvoltage. It is difficult to choose an optimal wavelet basis for the wavelet transform. In the S-transformation, the resolution of the high-frequency domain of the signal will be reduced, and the time-frequency analysis ability of the signal containing similar high-frequency components is poor because of the width of the Gaussian window to be the reciprocal of frequency. On the other hand, EMD has the problems of modal aliasing and endpoint effects [9]. As for the overvoltage signals with different time scales, the decomposed components are not unique, so that the adaptability of the method needs to be improved. In addition, there are much redundant information and high feature dimensions in the sub-signals decomposed by the above methods, which are not conducive to the recognition of subsequent classifiers. Therefore, it is necessary to investigate appropriate mathematical methods for dimensionality reduction to construct characteristics with low dimensionality and high discrimination information as the input features for pattern recognition. Traditional methods for feature dimensionality reduction include statistical analysis [10], [11], kernel principal component analysis [12], singular value decomposition [13], etc.

After key features are extracted, it is necessary to select an appropriate pattern recognition method for the overvoltage classification. In general, conventional methods include support vector machine (SVM) [14], artificial neural network [1], [15], fuzzy logic [16], deep learning [17], etc. Among them, SVM can obtain a high recognition accuracy in a small sample. Babu and Mohan [8] used RBF-SVM to classify three fault features, and compared the accuracy of extracted features using voltage waveforms at each phase. Experimental results in [8] showed that the recognition accuracy of each voltage signal was all over 92% through the trained network. In recent years, deep learning has been rapidly developed. Chen *et al.* [17] applied an automatic encoder to the identification of overvoltage. Without decomposing the signal, the overvoltage waveform was directly inputted into a neural network, and the feature was automatically extracted and identified. Although classifier-based methods have achieved extremely high accuracy, these classifiers either require a large amount of tagged data, or require tedious network hyper-parameters adjustment and training in advance, which takes a lot of time and is not easy for practical applications. Because the source of the overvoltage waveform is difficult to obtain, numerical simulations are generally used to train the corresponding model. When new measured data is added, diagnostic models need to be retrained. The entire diagnostic model is always operated under the process of training, diagnosis, labeling, and retraining.

This study proposes an internal overvoltage identification method based on time-frequency atomic decomposition. The atomic decomposition algorithm is different from Fourier transform, Wavelet transform, and other analytical methods that attempt to express signals with fixed basis functions. From the intrinsic properties of the signal, the adaptively selects the best matching atom in the over-complete atomic library to achieve signal expression. It is simple, flexible, and has a clear physical meaning. At present, this method has been widely used in many areas such as biomedical [18], speech and language analysis [19], etc. Yang *et al.* [20] first applied the atomic decomposition to solve the problem of the mixed overvoltage to be difficult for decomposing into a single overvoltage combination. In this study, the atomic decomposition algorithm is used to decompose seven types of internal overvoltage waveforms. After obtaining and constructing the effective and discriminant atom features, the identification can be completed only by thresholds. The proposed method has high recognition accuracy and strong adaptability through ATP/EMTP simulation, and actual data verification. Compared with traditional classifier-based identification methods, the proposed algorithm is easier to deploy in practical applications.

This study is organized into seven sections. Following the Introduction, Section II introduces the principle of atomic decomposition algorithm and its implementation process. Section III explains the source and characteristics of the overvoltage waveform. Section IV presents the feature extraction and recognition based on the atomic decomposition algorithm. Section V analyzes and discusses the experimental process and verification results. Section VI expresses

the application of the proposed method in a real system. Section VII summarizes the proposed method.

II. METHODOLOGY

A. ATOMIC DECOMPOSITION ALGORITHM

The implementation of atomic decomposition is based on matching pursuit (MP) [21]. After traversing the entire atomic library in each iteration, it will search out the atom to mostly match the current signal, and remove the corresponding atom from the original signal. Then, it traverses the atomic library again with the residual signal. When the number of iterations is reached, or the residual signal energy is lower than the preset threshold, the matching in this process will be stopped. Ultimately, the intrinsic characteristics of the signal can be linearly represented by these most matching atoms.

The most matching between the obtained atom and the signal in each iteration can be expressed as follows. Suppose that the atomic library is D and the signal is f. At the n^{th} iteration, the atom $g_{\gamma n}$ selected from D should have the largest inner product with the current residual signal $R^{n-1}f$, that is,

$$\begin{cases} R^0 f = f \\ R^n f = R^{n-1} f - \left\langle R^{n-1} f, g_{\gamma n} \right\rangle g_{\gamma n} \\ g_{\gamma n} = \arg\max\limits_{g_{\gamma i} \in D} \left| \left\langle R^{n-1} f, g_{\gamma i} \right\rangle \right| \end{cases} \tag{1}$$

where $R^0 f$ is the original signal, $R^n f$ is the residual component after the n^{th} iteration, $<, >$ is the inner product. After the n^{th} iteration, the signal f can be expressed as

$$f = \sum_{i=0}^{n-1} \left\langle R^i f, g_{\gamma i} \right\rangle g_{\gamma i} + R^n f \tag{2}$$

If the residual component $R^n f$ is assumed to be ignored, the signal can be approximated as

$$f = \sum_{i=0}^{n-1} \left\langle R^i f, g_{\gamma i} \right\rangle g_{\gamma i} \tag{3}$$

B. MP ALGORITHM BASED ON OPTIMIZATION

In the atomic decomposition algorithm, the choice of atomic library determines the efficiency of the algorithm, and the simplicity of the result. Since the overvoltage signal can be generally composed of fundamental superimposed harmonics or attenuated harmonic components, the attenuation sinusoidal model in [22] is used in this study, and can be expressed as

$$g_\gamma(t) = K_\gamma \left[u(t - t_s) - u(t - t_e)\right] e^{-\rho(t - t_s)} \cdot \cos(2\pi f t + \phi) \tag{4}$$

where $\gamma = (f, \rho, \phi, t_s, t_e)$ is the set of atomic five parameters, in which f is the frequency; ρ is the attenuation coefficient; ϕ is the phase; t_s and t_e are the starting and ending times, respectively; $u(t)$ is the unit-step function; K_γ is the normalization factor.

Every iteration of the MP algorithm needs to find atomic parameters to make the atom for matching the current signal best, which is essentially a 5-dimensional optimization problem. Therefore, an imperialist competitive algorithm (ICA) is selected to optimize the search process of the MP Algorithm. The ICA is a global optimization algorithm that draws on the competition between the empire of the colonial stage of human politics and the occupation of its colonies. The detailed principle of the algorithm can be referred to [23]. In order to solve the parameter optimization problem, it is assumed that the signal length to be decomposed is N, and the atomic parameter set $\gamma = (f, \rho, \phi, t_s, t_e)$ is discretized. The atomic parameter set can be rewritten as $\gamma = (2\pi f/N, 2\pi s/N, m/N, n_s, n_e)$, where $f \in [1, N]$, $s \in [0, N-1]$, $m \in [-N, N]$, and $0 \le n_s < n_e \le N-1$. The objective function can be defined as $\max F(f, s, m, n_s, n_e) = \left|\left\langle R^n x, g_{\gamma_n} \right\rangle g_{\gamma_n}\right|$. The process of searching the most matching atom by the ICA optimization algorithm is depicted in Fig. 1.

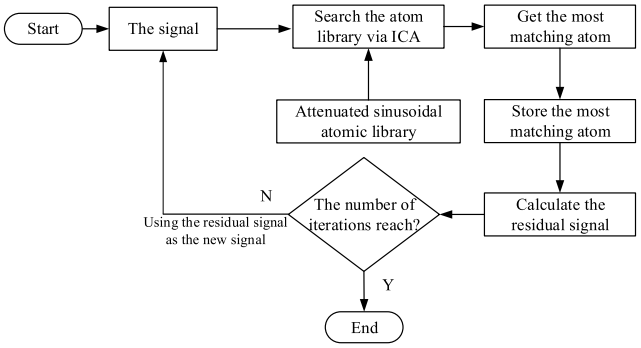

FIGURE 1. Flow chart of atomic decomposition algorithm.

A test signal $x(t)$ is constructed in (5) to verify the performance of the atomic decomposition algorithm.

$$x(t) = v(t) + \begin{cases} 10\cos(100\pi t), & 0 \le t \le 90\text{ms} \\ 12\cos(200\pi t)e^{-20t}, & 20 \le t \le 60\text{ms} \\ 14\cos(500\pi t), & 20 \le t \le 90\text{ms} \end{cases} \tag{5}$$

where $v(t)$ is the white noise with 20dB, which is used to test the noise immunity of the method. The sampling rate is 200kHz; the number of sampling points and iterations (n) are selected as 18000 and 4, respectively. The parameters of the obtained atoms are summarized in Table 1, where P_i is equal to $\left|\left\langle R^i x, g_{\gamma_i} \right\rangle\right|$ represents the matching degree between the atom and the original signal. Obviously, a larger value indicates that the atom matches the original signal better. The atom with the largest P_i (that is P_1) is defined as the dominant atom, which represents the original signal most. It can be seen that the first three atoms with larger P_i accurately identify the parameters such as the frequency, starting and ending times, and the attenuation factor of the three components contained in the original signal. Because P_i is very low for the fourth atom, the matching degree of the atom to the original signal is low, and it is called the false atom. Although the matching degree of the atom to the signal can be determined by the size of P_i, the value is related to the amplitude of the original signal, and it is difficult to directly use for excluding

TABLE 1. Parameters of most matching atom.

No.	P_i	f/Hz	t_s /ms	t_e /ms	ϕ /rad	ρ
1	1171.05	250.05	20.00	90.00	0.00	0.00
2	950.01	49.99	0.00	90.00	0.00	0.00
3	359.57	100.01	20.00	60.00	6.28	20.79
4	20.05	253.59	41.88	90.00	6.28	0.00

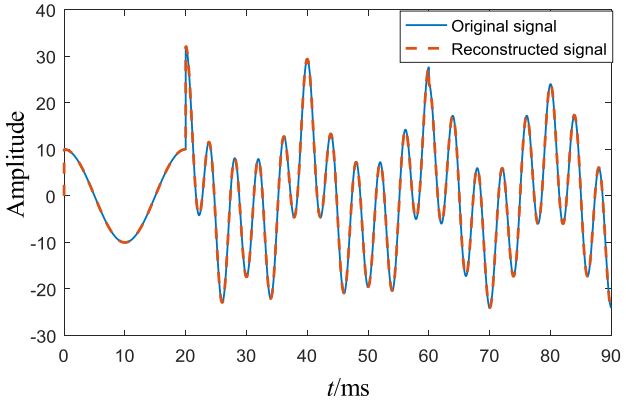

FIGURE 2. Comparison of original noiseless signal and reconstructed signal.

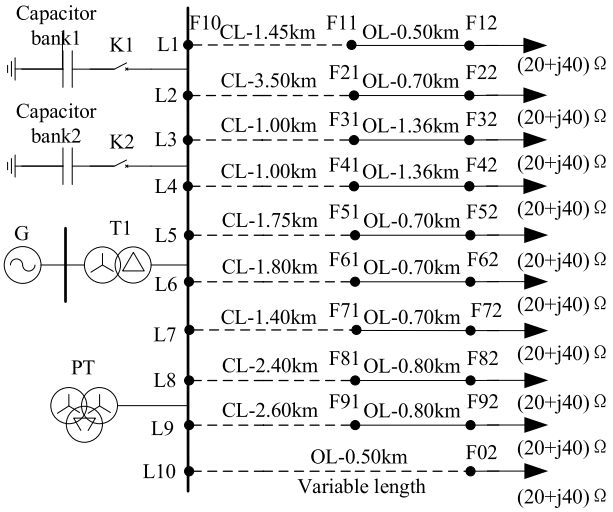

FIGURE 3. Simulation model of distribution network.

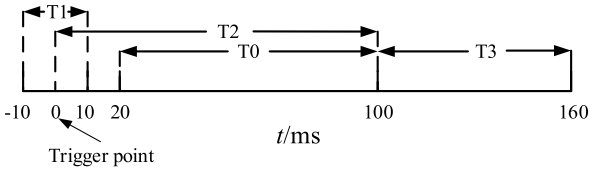

FIGURE 4. Period division of overvoltage signal.

the false atom. To solve this problem, the relative matching degree of the atom is defined as

$$G_i = P_i/P_1 \tag{6}$$

When the value (G_i) of an atom is very small, the atom can be ignored. As for the value (G_i) of the 4th atom equal to 0.017, since the value is too small, it is considered to be a false atom and can be ignored. The first to third atoms are combined for linear reconstruction, and the reconstructed waveform is basically consistent with the original noiseless waveform (as shown in Fig. 2). It shows that the atomic decomposition algorithm can not only restore the signal components to a certain extent, but also obtain the signal parameters.

III. WAVEFORM ACQUISITION AND ANALYSIS

In this study, the alternative-transients-program/electromagnetic-transients-program (ATP/EMTP) simulation software is used to build a distribution network model, and the corresponding overvoltage simulation waveform can be obtained for characteristic analyses and technical verification. The model is mainly built based on the basic data of a substation in Fujian Province, China, as shown in Fig. 3. In Fig. 3, T1 is a 110kV/10kV main transformer; the 10kV side is a neutral-point-ungrounded system, in which there are 10 feeders; OL and CL stands for the overhead line and the cable line, respectively; parameters of the transformer and these lines are the same as the ones in [24]; F10 to F92 are fault points; there are two sets of capacitors on the bus bar, in which each set with a capacity of 4200 kvar; K1 and K2 are time-controlled switches, in which the power-frequency is 50Hz, and the sampling rate is 200 kHz. Moreover, the length of the 10th line is variable, and the ferroresonance overvoltage is generated by changing the distance from the fault point F02 to the bus bar.

This model is used to generate seven types of internal overvoltage waveforms as the sample set including the single phase-to-ground type, the intermittent arc grounding type, the sub-frequency ferroresonance type, the fundamental ferroresonance type, the high-frequency ferroresonance type, the capacitor switching type, and the line switching type. In general, the overvoltage monitoring system triggers the sampling device after the overvoltage occurs, and records the waveform before and after the overvoltage [7]. In this study, the voltage waveform from the 0.5 cycle before the trigger to the 8 cycle after the trigger (time range is -10ms∼160ms) is taken as the target signal, and the signal is divided into four time periods, named T0∼T3, as shown in Fig. 4. As for the difference of different overvoltage waveforms characteristics in different time periods, key features can be extracted.

The temporary overvoltage lasts for a long time, and the three-phase voltage waveforms of the single phase-to-ground type are depicted in Fig. 5(a). The amplitude of the faulty phase voltage drops to 0 after experiencing a short high-frequency oscillation, and the amplitude of the normal phase voltage increases to $\sqrt{3}$ times of the original value. Although intermittent arc grounding is an operating overvoltage, it is classified as transient overvoltage because of its long duration. Their three-phase voltage waveforms are depicted in Fig. 5(b). During the faulty period, three-phase voltage

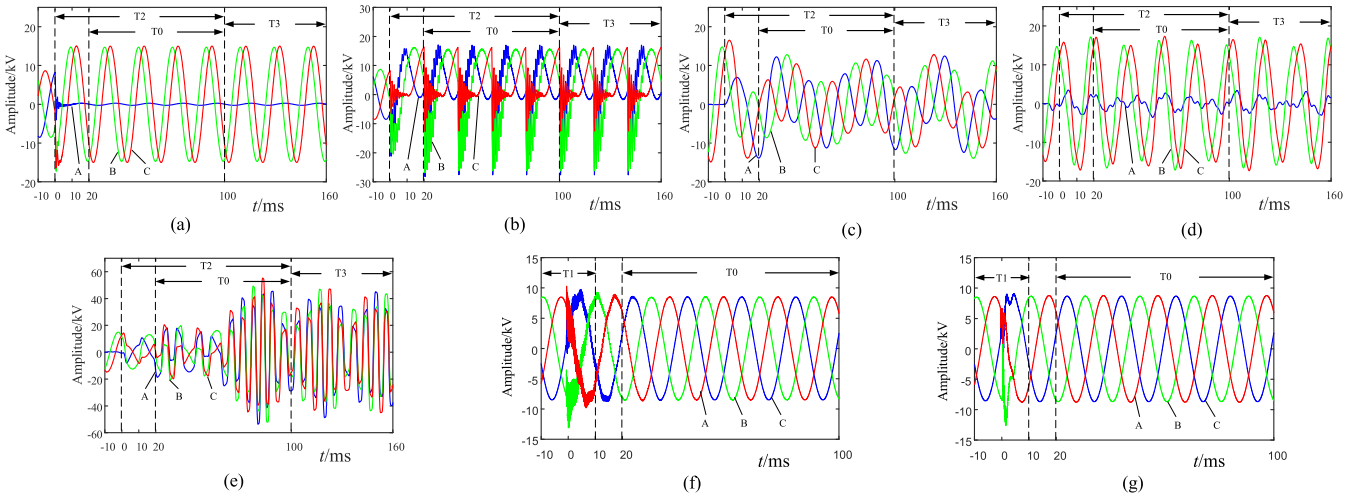

FIGURE 5. Waveforms of overvoltage. (a)Single phase-to-ground; (b) Intermittent arc grounding; (c) Sub-frequency ferroresonance; (d) Fundamental ferroresonance; (e) High-frequency ferroresonance; (f) Line switching; (g) Capacitor switching.

waveforms are seriously distorted due to the multiple ignition and extinguishing of the fault phase, and high-frequency components are generated on three-phase voltages. Ferroresonance mainly includes sub-frequency, fundamental and high-frequency. The corresponding waveforms are depicted in Fig. 5(c), 5(d) and 5(e), respectively. Ferroresonance is excited at 20ms, and the main frequencies of waveform signals of the fundamental, sub-frequency, and high-frequency ferroresonance are power-frequency, fractional multiple of power-frequency, and integer multiple of power-frequency, respectively. In addition, the overvoltage waveforms induced by the capacitor switching type and the line switching type are depicted in Fig. 5(f) and 5(g), respectively.

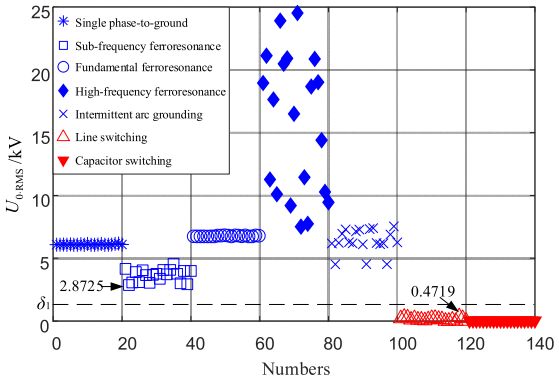

FIGURE 6. Distribution of $U_{0\cdot RMS}$.

IV. IDENTIFICATION OF OVERVOLTAGE

In this study, a novel internal-voltage overvoltage identification method for a distribution network is investigated. It mainly uses four parameters (f, t_s, t_e, G_i) of several atoms obtained by the atomic decomposition to construct key features, and forms five criteria for the overvoltage identification. The number of iterations of all atomic decompositions is uniformly set to be 10, so that not only effective atoms but also some false atoms can be obtained. In addition, only the atoms with G_i greater than 0.05 are considered. If the value of G_i is too small, it can be considered as noise. By the selection in this study, it can cover most of 95% waveform information when the relative matching value is 5%.

A. TIME-DOMAIN FEATURE EXTRACTION

The duration of the operating overvoltage is much shorter than that of the temporary overvoltage, lasting only about 10ms [2]. In other words, in the T0 period, the operating overvoltage has been restored to normal, and the relatively complete information of sub-frequency ferroresonance can be obtained with the duration of four cycles. Therefore, the root-mean-square (RMS) value of the zero-sequence voltage in the T0 period ($U_{0\cdot RMS}$) can be taken as the feature to distinguish the operating overvoltage from the temporary overvoltage, and the corresponding formula can be represented as

$$\begin{cases} U_0(n) = (U_A(n) + U_B(n) + U_C(n))/3 \\ U_{0\cdot RMS} = \sqrt{\dfrac{1}{N}\sum_{n=1}^{N} U_0^2(n)} \end{cases} \tag{7}$$

where $U_A(n)$, $U_B(n)$ and $U_C(n)$ express the voltage sampling sequences of three-phase voltages; $U_0(n)$ is a sampling sequence of the zero-sequence voltage; N is the sampling number of four cycles.

In the simulation model, 140 overvoltage samples are obtained (i.e. 20 samples for each type), and then $U_{0\cdot RMS}$ can be calculated. The distribution of $U_{0\cdot RMS}$ is depicted in Fig. 6. As can be seen form Fig. 6, it is obvious that $U_{0\cdot RMS}$ for the operating overvoltage is lower than that for the temporary overvoltage. Therefore, **Criterion I** for the overvoltage identification can be defined as follows.

In the T0 period, when the value of $U_{0\cdot RMS}$ is less than the threshold value (δ_1), it can be judged as the operating overvoltage; otherwise, it can be judged as the temporary overvoltage.

The value of δ_1 must be taken into account to maximize the distinction between the operating overvoltage and the transient overvoltage. With respect to small sample distribution statistics (as shown in Fig. 6), the minimum value of $U_{0\cdot\mathrm{RMS}}$ for the temporary overvoltage is 2.8725kV, while the maximum value of $U_{0\cdot\mathrm{RMS}}$ for the operating overvoltage is 0.4719kV, and the distribution is relatively stable. Therefore, the value of δ_1 can be conservatively selected as 1.5kV.

B. FREQUENCY DOMAIN FEATURES EXTRACTION

1) FEATURE EXTRACTION IN T1 PERIOD

As mentioned above, the duration of the transient component for the operating overvoltage is generally less than 10ms, while the T1 period includes the characteristic information before and after the fault of the operating overvoltage. Therefore, this study uses the information of the T1 period to identify the overvoltage caused by line or capacitor switching. The atomic decomposition is performed on three-phase voltage waveforms during this period, and decomposed atomic parameters are used for identification.

According to the waveform analysis in section III, the duration of the line switching is longer than that of the capacitor switching. To reflect this difference, the duration of the atom at the frequency (f) is defined as

$$T(f) = t_e - t_s \tag{8}$$

where t_s and t_e are the starting time and the ending time of the atom, respectively. Yang *et al.* [25] stated that the time durations of the capacitor switching and the line switching to be about 2∼3ms and 10ms, respectively. By considering the difference of the waveform, the duration of 5ms is taken as the boundary value. The atomic decomposition is performed on 100 overvoltage samples including line and capacitor switching, and the frequency distribution for effective atom duration of A-phase waveform in two intervals greater than and less than 5ms is depicted in Fig. 7. As can be seen from Fig. 7, it is obvious that two overvoltage types have low-frequency and high-frequency components as $T \leq 5$ms, and the difference of the frequency characteristics is not significant. Fortunately, the atomic frequency difference as$T > 5$ms is sufficient to identify them. The reason is that the high-frequency oscillation of the capacitor switching has disappeared, resulting in the frequency of the effective atom to be less than 2000Hz. But, the line switching still has atoms over 2000Hz in this interval.

In some cases, the transient characteristics of one phase voltage may not be obvious, and the values of G_i for some atoms are too low, so that the effective atom cannot be successfully extracted. Therefore, **Criterion II** for the overvoltage identification can be defined as follows. In the T1 period, if there are atoms with the frequency to be greater than 2000Hz, and its duration is longer than 5ms in two-phase voltages, it can be judged as the overvoltage caused by the line switching. If there are atoms with the frequency to be less than 2000Hz, and its duration is less than 5ms in two-phase voltages, it can be judged as the overvoltage caused by the capacitor switching. Otherwise, it can be judged as another type of operating overvoltage.

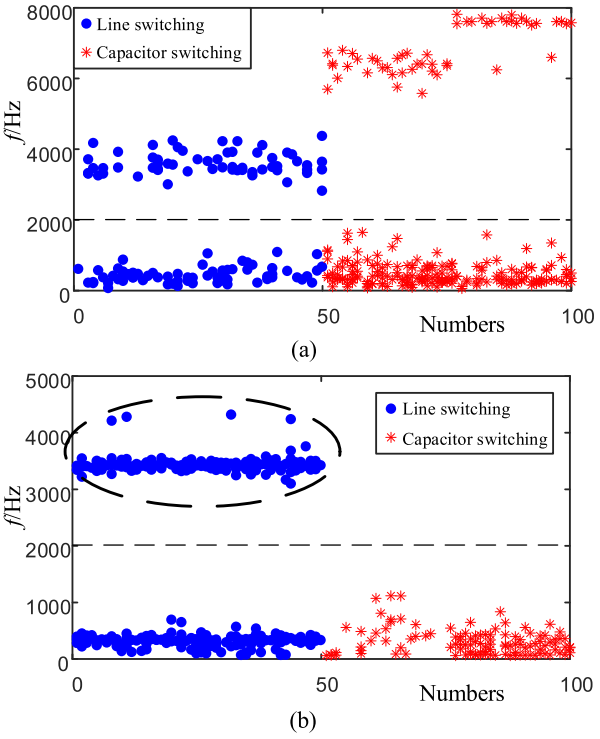

FIGURE 7. Frequency distribution of effective atomic frequency distribution in T1 period. (a) $T \leq 5$ms; (b) $T > 5$ms.

2) FEATURE EXTRACTION IN T2 PERIOD

In general, the duration of the temporary overvoltage is relatively long, including a certain transient process, and the signal gradually stabilizes over time. Moreover, the intermittent arc grounding overvoltage has a strong uncertainty in the duration, which may stabilize combustion or may extinguish the arc immediately. In order to obtain its information characteristics, the analysis period should not be set too long. The T2 period includes the transient and steady-state development phases of the overvoltage, and the duration of five cycles ensures the frequency characteristics of the sub-frequency ferroresonance and the intermittent arc grounding.

In order to study the frequency characteristics of five types of temporary overvoltage, the discrete fourier transform (DFT) is performed on their zero-sequence voltages, and the corresponding results are depicted in Fig. 8. It is shown that the ferroresonance at sub-frequency and high frequency are different from the other three types, and the maximum energy distribution is in the non-power-frequency band. With respect to this characteristic, two types of ferroresonance can be identified firstly.

The frequency of the high-frequency ferroresonance is distributed at integer multiple of 2, 3, 4, etc. of the power frequency, while that of the sub-frequency ferroresonance is mainly distributed at fractions of 1/2, 1/3, 1/4, etc. of the power frequency. Therefore, the dominant atoms of the

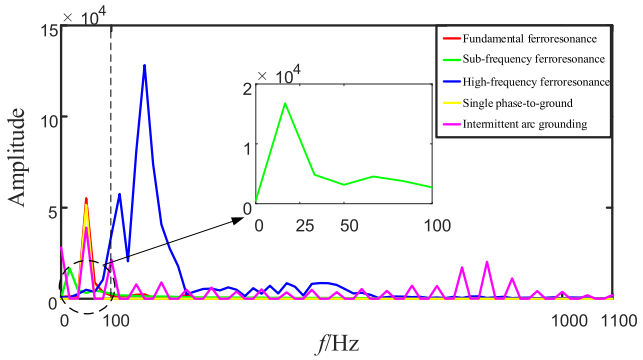

FIGURE 8. DFT analysis result of five types of overvoltage.

high-frequency and sub-frequency ferroresonance must have significant differences with the power-frequency overvoltage. **Criterion III** for the overvoltage identification can be defined as follows.

In the T2 period, if the frequency of the dominant atom is greater than 100Hz, it can be judged as the high-frequency ferroresonance. If the frequency of the dominant atom is less than 40 Hz, it can be judged as the sub-frequency. Otherwise, it is the power-frequency overvoltage.

Similarly, some phenomena also can be seen from Fig. 8. Among the power-frequency overvoltage, the intermittent arc grounding has a large number of harmonics with larger amplitudes in the frequency-band greater than 100 Hz, which is mainly due to the grounding phase with multiple burning and arcing. The transient frequency of the intermittent arc grounding is mainly distributed at 100∼3000Hz [26]. Therefore, the atomic frequency is in this frequency-band can be defined as the high-frequency atom, and the total relative matching degree of high-frequency atom reflecting the amount of high-frequency components contained in the waveform can be calculated as

$$G_{H\cdot toal} = \sum_{f=100}^{3000} G_f \tag{9}$$

where G_f is the relative matching degree of the atom of $f \in [100, 3000]$.

20 single phase-to-ground, fundamental ferroresonance, and intermittent arc grounding samples are selected, respectively. After the atomic decomposition, the value of $G_{H\cdot toal}$ at three types of overvoltage can be calculated and depicted in Fig. 9. It is obvious that the fundamental ferroresonance only has a small number of components larger than 100 Hz, and the value of $G_{H\cdot toal}$ is low due to the fewer atoms and low relative matching degree. Similarly, the value of $G_{H\cdot toal}$ for the single phase-to-ground type is also very low. However, when the single phase-to-ground occurs at certain phase angles, the value of $G_{H\cdot toal}$ at individual samples is higher due to short-term high-frequency oscillations. The value of $G_{H\cdot toal}$ at the intermittent arc grounding type is obviously higher than the other two types of overvoltage. Due to the influence of various external factors, the uncertainty of

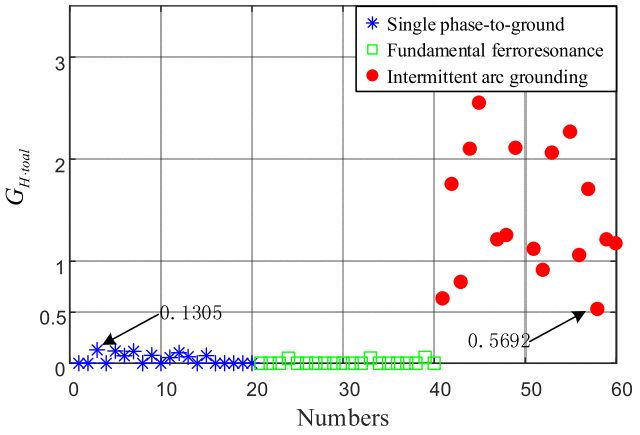

FIGURE 9. $G_{H\cdot toal}$ distribution in T2 period.

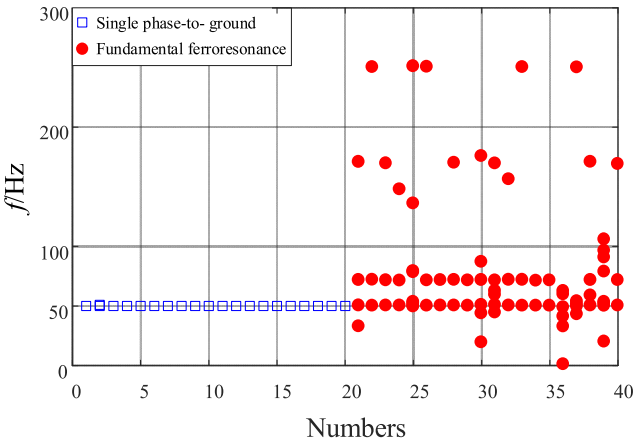

FIGURE 10. Frequency distribution of effective atom in T3 period.

ignition and arc extinction is large. Therefore, **Criterion IV** for the overvoltage identification can be defined as follows.

In the T2 period, if the value of $G_{H\cdot toal}$ is greater than the threshold value (δ_2), it can be judged as the intermittent arc grounding type. In Fig. 9, for the intermittent arc grounding, the minimum value of $G_{H\cdot toal}$ is equal to 0.5692, while for the single phase-to- ground and fundamental ferroresonance, the maximum value of $G_{H\cdot toal}$ is equal to 0.1305. Therefore, the value of δ_2 can be conservatively selected as 0.4.

3) FEATURE EXTRACTION IN T3 PERIOD

After 5 cycles under the occurrence of overvoltage, single phase-to-ground and fundamental ferroresonance have entered a stable state. The transient process of single phase-to-ground disappears, and the waveform is a stable power-frequency waveform. Moreover, the fundamental ferroresonance enters a stable oscillation state. Since the steady-state characteristics are more obvious, two types of overvoltage can be distinguished in the T3 period.

Similarly, 20 single phase-to-ground and fundamental ferroresonance samples are respectively selected, and the zero-sequence voltage in the T3 period can be decomposed. The frequency distribution of effective atoms is depicted in Fig. 10. Obviously, the single phase-to-ground has only one

TABLE 2. Experimental condition and identification results.

Type	Fault position / line length	Fault phase	Fault initial phase angle	Transition resistance	Samples	Accuracy
Single phase-to-ground	F21, F22, F41, F42, F82, F10	A,B,C	0°, 45°, 90°,135°, 180°,225°, 270°, 315°	1~20Ω	864	100%
Sub-frequency ferroresonance	1.3~20km,	A,B,C	0°, 45°, 90°,135°, 180°,225°, 270°, 315°	5Ω	330	100%
Fundamental ferroresonance	0.25~1.3km	A,B,C	0°, 45°, 90°,135°, 180°,225°, 270°, 315°	5Ω	330	97.27%
High-frequency ferroresonance	0.01~0.12km	A,B,C	0°, 45°, 90°,135°, 180°,225°, 270°, 315°	5Ω	330	100%
Capacitor switching	K1 or/and K2	A,B,C	30°, 60°, 90°,120°,150°,180°°,180° 210°,240°,270°,300°,330°	——	334	100%
Line switching	L1~L10	A,B,C	30°, 60°, 90°,120°,150°,180°°,180° 210°,240°,270°,300°,330°	——	344	100%
Intermittent arc grounding	F10, F61~F92	A,B,C	90°,270°	1~20Ω	210	100%

effective atom with a frequency of 50 Hz, while each sample of the fundamental ferroresonance under stable oscillation still contains some non-power-frequency atoms.

By considering the error of the decomposition result, **Criterion V** for the overvoltage identification can be defined as follows.

In the T3 period, if there is an atom, whose frequency satisfies the condition of $60 \leq f \leq 300$ Hz, it can be judged as the fundamental ferroresonance type. If all atomic frequencies satisfy the condition of $40 < f < 60$ Hz, it can be judged as the single phase-to-ground type.

C. IDENTIFICATION PROCESS

In this study, the features are extracted in the time domain and the frequency domain, and the overvoltage type can be hierarchically identified according to the identification criteria after the threshold values of δ_1 and δ_2 are predetermined. The steps are explained as follows.

Step 1: When an overvoltage occurs, three-phase voltage waveforms in the target period at the bus bar of the distribution network are recorded by the fault recorder.

Step 2: Calculate the value of $U_{0\cdot\mathrm{RMS}}$ in the T0 period, and identify the operating overvoltage (next to step 3) or the temporary overvoltage (next to step 4) by Criterion I.

Step 3: For the operating overvoltage, atomic decomposition is performed on the three-phase voltage waveforms during the T1 period to obtain high-frequency effective atoms and their duration. The overvoltage of the line switching or the capacitor switching can be recognized by Criterion II.

Step 4: For the transient overvoltage, the zero-sequence voltage during the T2 period is decomposed to calculate the frequency of the dominant atom, and the high-frequency ferroresonance, sub-frequency ferroresonance, or power-frequency overvoltage can be identified by Criterion III (next to step 5).

Step 5: For the power-frequency overvoltage, the total relative matching degree of high-frequency atoms during the T2 period is calculated, and the intermittent arc grounding overvoltage or the remaining two types can be identified by Criterion IV (next to step 6).

Step 6: The frequency distribution of the effective atom of the zero-sequence voltage during the T3 period is calculated, and the fundamental ferroresonance or single phase-to-ground overvoltage can be identified by Criterion V.

The detailed process is depicted in Fig. 11, where $f_{1\mathrm{A}}^{m}$, $f_{1\mathrm{B}}^{p}$,$f_{1\mathrm{C}}^{q}$ respectively express the atomic frequencies for three-phase voltages A, B and C in the T1 period, and take A-phase and B-phase as examples to represent any two phases in the three-phase system; m, p, q, k, and l denote the number of atoms; f_2^k and f_3^l denote the atomic frequencies in the T2 and T3 periods, respectively.

V. EXPERIMENT AND DISCUSSION

A. ACCURACY ANALYSIS

Various types of overvoltage samples can be obtained from the simulation model in Fig. 3 to verify the effectiveness of the proposed method. By changing faulty phase angle, phase separation, closing time, and other factors, 2742 overvoltage samples (Data 1) are obtained in Table 2, in which the sampling rate is set as 200 kHz. Especially, for the single phase-to-ground, the variation of transition resistance is from 1Ω to 20Ω. Two threshold parameters (δ_1 and δ_2) are set as 1.5kV and 0.4, respectively.

All the samples are used for the verification of the proposed method. From the identification results, the recognition accuracy of the overvoltage type is 100%, except for the fundamental ferroresonance. There are two reasons. Firstly, the extracted characteristic frequency is not the main component and may be interfered by the errors.

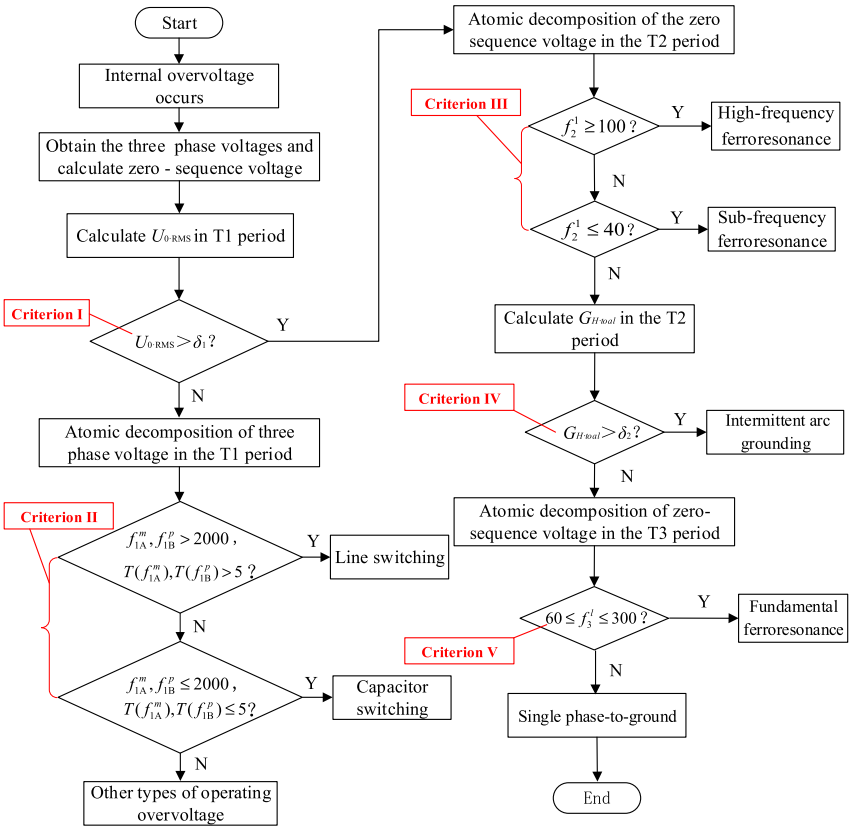

FIGURE 11. Flow of overvoltage identification based on atomic decomposition algorithm.

Secondly, the fault location also affects the content of the characteristic frequency. When the fault location is close to the oscillation range of the sub-frequency ferroresonance, the content of characteristic frequency will be further reduced. It may lead to the decrease of atomic relative matching degree for some samples and the misjudgment of single phase-to-ground. Nevertheless, the recognition accuracy of the fundamental ferroresonance still can reach 97.27%, and the overall recognition accuracy of overvoltage can achieve 99.89%, which indicates that the proposed algorithm can effectively identify seven types of overvoltage.

B. ADAPTIVE ANALYSIS

1) ANTI-INTERFERENCE CAPABILITY

Since there may be a lot of noise in the actual field, it is necessary to verify whether the algorithm can identify effectively under noise interference. 20% of the correctly identified samples in Table 2 are randomly selected as the analysis sample (Data 2), which was added into 20dB Gaussian white noise for recognition. The corresponding recognition results are summarized in Table 3. It is clearly seen that although the recognition accuracy is reduced after adding noise, it still can reach 99.63%. Because the recognition criteria mainly involve dominant atom or the atoms with a large relative matching degree, the algorithm has a strong anti-noise performance.

TABLE 3. Recognition accuracies under noise interference.

Type	Samples	Accuracy	
		Non-noise	Noise
Single phase-to-ground	172	100%	100%
Sub-frequency ferroresonance	66	100%	100%
Fundamental ferroresonance	66	100%	100%
High-frequency ferroresonance	66	100%	100%
Capacitor switching	66	100%	96.97%
Line switching	68	100%	100%
Intermittent arc grounding	42	100%	100%
Total	546	100%	99.63%

2) SAMPLING OUT OF SYNCRONIZATION

The overvoltage recording device may appear three-phase asynchrony when collecting waveforms. In order to study the influence of signal sampling asynchrony on diagnosis accuracy, the C-phase voltage is set to lag the A-phase voltage by 0.1ms at the sampling time, and the Data 2 samples are processed for correlation. The recognition results are summarized in Table 4. It is shown that the identification method is

TABLE 4. Recognition accuracies under asynchronous sampling.

Type	Samples	Accuracy
Single phase-to-ground	172	100%
Sub-frequency ferroresonance	66	100%
Fundamental ferroresonance	66	98.48%
High-frequency ferroresonance	66	100%
Capacitor switching	66	100%
Line switching	68	100%
Intermittent arc grounding	42	100%
Total	546	99.82%

TABLE 5. Recognition accuracies under different sampling rates.

Type	Samples	Accuracy	
		16kHz	4kHz
Single phase-to-ground	172	100%	100%
Sub-frequency ferroresonance	66	100%	100%
Fundamental ferroresonance	66	100%	100%
High-frequency ferroresonance	66	100%	100%
Capacitor switching	66	100%	100%
Line switching	68	98.53%	0%
Intermittent arc grounding	42	100%	97.62%
Total	546	99.82%	87.36%

basically not affected by the sampling out of synchronization, and can still effectively identify seven types of overvoltage.

3) DIAGNOSIS AT LOW SAMPLING RATE

In order to collect operating overvoltage waveforms, some data recorders typically operate at higher sampling rates, e.g. 200 kHz. But high sampling rates represent a high cost of equipment and a large software resource overhead. In order to verify the effectiveness of the proposed method at a low sampling rate, the samples of Data 2 with low sampling rates 16kHz and 4kHz are examined. The recognition results are summarized in Table 5.

Comparing the recognition results under two sampling rates, the method can effectively identify overvoltage types at the sampling rate of 16 kHz, and the accuracy is over 98.53%. However, at the sampling rate of 4 kHz, one sample of the intermittent arc grounding is misjudged due to the reduction of the high-frequency component of the waveform. Similarly, the line switching is not recognized because the effective frequency of the waveform acquired at this sampling rate to be less than 2000 Hz required for the fault identification. As can be seen from Fig. 7(a), the effective atomic frequency of the capacitor switching is up to 8 kHz. If two types of operating overvoltage are effectively recognized, the waveform sampling rate should be not less than 16 kHz.

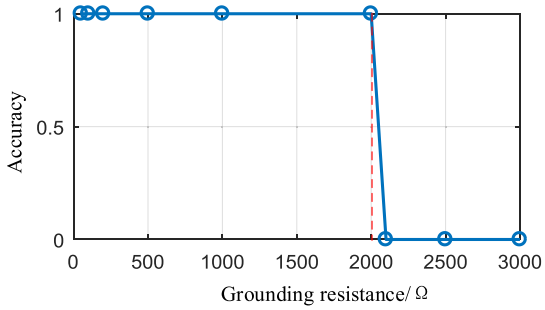

FIGURE 12. Diagnosis results under different grounding resistances.

4) HIGH-RESISTANCE GROUNDING FAULT DIAGNOSIS

In general, there are two types of single phase-to-ground including the low-resistance grounding and the high-resistance grounding. Since the high overvoltage amplitude is easily generated by the low-resistance grounding, metallic-to-ground overvoltage is generally considered in the overvoltage identification. However, the high-resistance grounding faults often occur in the distribution network, especially in the early stage of insulation damage. Its characteristics are that the non-fault phase voltage amplitude will not rise very high, and the fault phase waveform is very different from the metallic-to-ground. If the features are still constructed with respect to the characteristic of the faulty phase amplitude close to zero [7], it will be difficult to identify the high-resistance grounding fault.

In this study, the proposed method is applied to fault identification with the high-resistance grounding, and its applicable range is evaluated. Numerical simulations at the high-resistance grounding are performed in the fault point F10∼F12 of the model in Fig. 3. The initial phase angles of the fault are 0°, 45°, and 90°, respectively. The grounding resistance values are 50, 100, 200, 500, 1000, 2000, 2100, 2500, 3000Ω. There are 81 samples, and the recognition results are depicted in Fig. 12.

When the grounding resistance is less than 2000 Ω, the proposed method can effectively identify. If the grounding resistance exceeds 2000 Ω, it cannot be recognized because the RMS value of the zero-sequence voltage is lower than the threshold value (δ_1). In fact, the increase of the grounding resistance only changes the amplitude of the fault phase, and it does not change the frequency component of the zero-sequence voltage. Since the proposed method is based on the difference in frequency between the single phase-to-ground and the fundamental ferroresonance, it can be effectively identified when the grounding-resistance is from 0 to 2000 Ω.

C. DISCUSSION

Numerical simulations show that the proposed method has high recognition accuracy and adaptability. Methods in other literatures are compared from three aspects of feature extraction, data requirements, and computational complexity.

Wang *et al.* [7] extracted six features by the S-transformation of phase voltages, in which the temporary overvoltage can be represented by a single dimension feature, and the operating overvoltage and lightning overvoltage can be represented by 5-dimensional features. Due to different expressive abilities of these features, fuzzy expert system and support vector machine (SVM) were trained for identification. Chen *et al.* [17] used the single-layer auto-encoder (SAE) and the stack sparse auto-encoder (SSAE) to reduce the dimensional and feature extraction of the three-phase voltage waveform. However, the obtained features have no physical meaning or interpretation. Lin *et al.* [27] adopted wavelet to decompose the signal into different frequency bands and extracted 36 features for identification. The frequency band of the wavelet decomposition can only be divided by a multiple of 2 according to the sampling rate, and these frequency bands cannot be artificially adjusted. Therefore, 36 features were extracted to describe the overvoltage characteristics, and the multi-level SVM was used for identification. In this study, atomic decomposition is used to obtain a plurality of atomic signals for matching the original waveform best. Each atomic signal contains five information parameters with practical physical meanings, which can help fault analysis and overvoltage suppression.

Whether it is a fuzzy expert system, SVM or softmax, it is a classifier for supervised learning. If one wants to train a good performance identification network, a sufficient number of training samples is always required. If the dimension of data is large, dimensionality reduction optimization should also be considered to solve the problem of over-fitting or local optimal. Thus, this kind of method is not suitable for the field of small sample identification. According to the characteristics of overvoltage signals, this study achieves a low-dimensional representation of features with a high degree of feature discrimination. Only a small amount of labeled measured data or simulated data is required to obtain reliable thresholds, which does not require network training. Therefore, it is relatively easy to realize the deployment and application.

In terms of computational complexity, the calculation of S-transformation is relatively large, and SAE and SSAE networks are also relatively complex. The tuning process requires high performance of the computer, while the atomic decomposition and wavelet transform are relatively simple. Ordinary computers or embedded systems can complete the corresponding work.

Performance comparisons with other published papers [7], [17], [27] are given in Table 6. Although the identification accuracy of these four methods is very close, the advantages of the proposed method are obviously recited as follows: (1) Features with physical meaning; (2) Unnecessary of classifier training; (3) Low requirement for hardware devices.

TABLE 6. Performance comparison.

System	Feature extraction	Computational complexity	Classifier	Accuracy
Proposed method	Atomic decomposition	Small	Rule-based Fuzzy Expert System & SVM	99.89%
Ref. [7]	S-transform	Large		97.8%
Ref. [17]	SAE & SSAE	Large	Softmax	97.0%
Ref. [27]	Wavelet transform	Small	SVM	98.28%

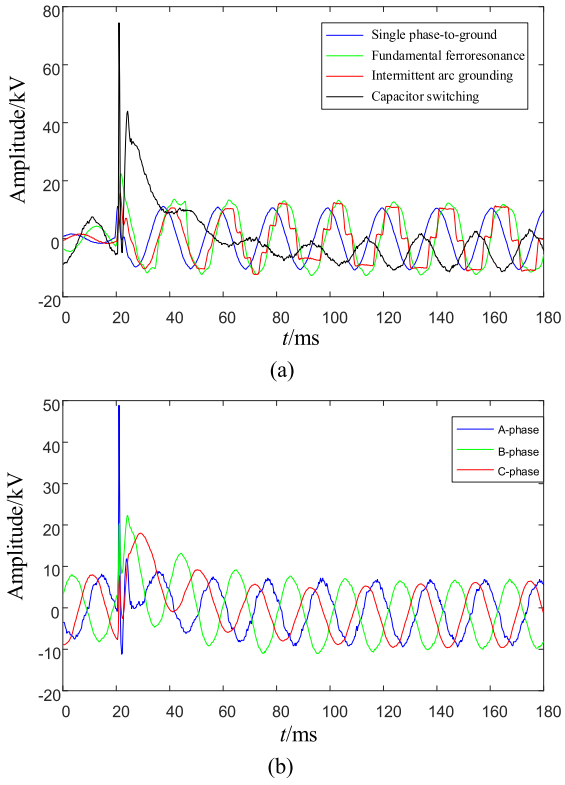

FIGURE 13. Voltage waveform measured by fault indicator. (a) Waveforms of zero-sequence voltage; (b) Three-phase voltage waveforms of capacitor switching.

VI. APPLICATIONS

In many countries and regions, feeder monitoring terminals and fault indicators for faulty line selection and faulty location have been widely applied in the field of smart distribution networks. Because of low cost, convenient installation, and flexible communication mode, the fault indicator with transient waveform recording is favored by power-grid users. In this study, the fault indicator with transient waveform recording is used to diagnose the type of overvoltage.

When a fault occurs in the circuit, the fault indicator of each phase is triggered and started to record three-phase voltage and current waveforms before and after the fault, which are synthesized by the collection unit to generate zero-sequence waveforms and upload all waveforms to the main station. In fact, the fault indicator cannot really collect the phase voltage. Instead, it can obtain the change of the ground electric field in the form of capacitor partial voltage to represent the transient change characteristics of the voltage waveform. Therefore, there are some differences between the so-called electric field waveform and the

TABLE 7. Diagnosis results by measured signals.

Type	Samples	Correct
Single phase-to-ground	4	4
Fundamental ferroresonance	7	6
Intermittent arc grounding	6	5
Capacitor switching	1	1
Accuracy	88.89%	

actual voltage waveform, which makes it difficult to diagnose various types of overvoltage. Since the fault indicator is separately phase-recorded, there is inevitably a three-phase asynchronous problem. Fortunately, as far as the equipment manufacturing standard is concerned, the synchronous sampling error of the three-phase waveform is not more than 0.1ms. In other words, the performance of the proposed method is not affected by the sampling out of synchronization problem according to the previous analysis. The fault indicator always has a sampling rate of 4 kHz because of the working power supply. Therefore, in addition to the overvoltage of line switching, other six types of overvoltage can be theoretically recognized. Fig. 13 shows the voltage waveforms of the single phase-to-ground, the fundamental ferroresonance, the intermittent arc grounding, and the capacitor switching collected by the fault indicator.

It is clearly seen that waveforms of the single phase-to-ground and the fundamental ferroresonance are similar to the simulated waveform. The high-frequency component of the intermittent arc grounding is significantly reduced due to the reduced sampling rate. The waveform of the capacitor switching is more intense with respect to the simulated waveform and occurs the low-frequency oscillation. In order to verify the identification ability to the voltage waveform collected by the fault indicator, 18 sets of measured overvoltage signals are selected for verification. The recognition results are summarized in Table 7, which clearly indicates that the recognition accuracy of the single phase-to-ground and the capacitor switching are 100%, and the intermittent arc grounding and the fundamental ferroresonance have only one sample to be misjudged. The reason for the misjudgment of the intermittent arc grounding samples is that the high-frequency components of the waveform collected by the fault indicator are insufficient, resulting in the total relative matching degree in the T2 period to be lower than the threshold value. With the improvement of the waveform sampling precision of the equipment, this problem will be solved. The sample of fundamental ferroresonance is misjudged as the single phase-to-ground because the content of power-frequency component is slightly higher than the threshold value. In practice, the threshold value can be re-adjusted according to the measured data. Although the number of measured samples is small, the total recognition accuracy still can reach 88.89%.

VII. CONCLUSION

This study investigates an internal overvoltage identification method for distribution networks. The effective atoms and their parameter information can be obtained by time-frequency atomic decomposition. The parameters with low dimension, physical meaning, and high discrimination are used as key features. Moreover, five identification criteria are designed, which can be used to distinguish seven types of overvoltage without training the classifier. Since the proposed method requires less computing resources, it is easy to deploy in the device terminal. This study further verifies that the proposed method has strong adaptability and high recognition accuracy in numerical simulations and measured data. The proposed method can achieve the accuracy improvements 2.09%, 2.89% and 1.61% than [7], [17] and [27], respectively. Even for experimental data, the recognition accuracy of the proposed method also can be over 88%.

REFERENCES

[1] H. Chen, P. D. S. Assala, Y. Cai, and P. Yang, "Intelligent transient overvoltages location in distribution systems using wavelet packet decomposition and general regression neural networks," *IEEE Trans. Ind. Inf.*, vol. 12, no. 5, pp. 1726–1735, Oct. 2016.

[2] W. Sima, H. Zhang, M. Yang, T. Yuan, P. Sun, Q. Chen, and H. Zhao, "A framework for automatically cleansing overvoltage data measured from transmission and distribution systems," *Int. J. Elect. Power Energy Syst.*, vol. 102, pp. 381–392, Nov. 2018.

[3] X. Qin, P. Wang, Y. Liu, G. Sheng, and X. Jiang, "Research on distribution network fault recognition method based on time-frequency characteristics of fault waveforms," *IEEE Access*, vol. 6, pp. 7291–7300, 2018.

[4] L. Angrisani, P. Daponte, M. D'Apuzzo, and A. Testa, "A measurement method based on the wavelet transform for power quality analysis," *IEEE Trans. Power Del.*, vol. 13, no. 4, pp. 990–998, Oct. 1998.

[5] G. Mokryani, M. R. Haghifam, and J. Esmaeilpoor, "Identification of ferroresonance based on wavelet transform and artificial neural network," *Eur. Trans. Elect. Power*, vol. 19, no. 3, pp. 474–486, Apr. 2009.

[6] Y. Q. Chen, O. Fink, and G. Sansavini, "Combined fault location and classification for power transmission lines fault diagnosis with integrated feature extraction," *IEEE Trans. Ind. Electron.*, vol. 65, no. 1, pp. 561–569, Jan. 2018.

[7] J. Wang, Q. Yang, W. Sima, T. Yuan, and M. Zahn, "A smart online overvoltage monitoring and identification system," *Energies*, vol. 4, no. 4, pp. 599–615, Apr. 2011.

[8] N. R. Babu and B. J. Mohan, "Fault classification in power systems using EMD and SVM," *Ain Shams Eng. J.*, vol. 8, no. 2, pp. 103–111, Jun. 2017.

[9] Z. J. Wang, J. Zhou, J. Wang, W. Du, J. Wang, X. Han, and G. He, "A novel fault diagnosis method of gearbox based on maximum kurtosis spectral entropy deconvolution," *IEEE Access*, vol. 7, pp. 29520–29532, 2019.

[10] X. Zhao, C. Yao, Z. Zhao, and A. Abu-Siada, "Performance evaluation of online transformer internal fault detection based on transient overvoltage signals," *IEEE Trans. Dielectr. Electr. Insul.*, vol. 24, no. 6, pp. 3906–3915, Dec. 2017.

[11] M. Yang, W. Sima, Q. Yang, J. Li, M. Zou, and Q. Duan, "Non-linear characteristic quantity extraction of ferroresonance overvoltage time series," *IET Gener., Transmiss. Distrib.*, vol. 11, no. 6, pp. 1427–1433, Apr. 2017.

[12] G. Mokryani, P. Siano, and A. Piccolo, "Identification of ferroresonance based on S-transform and support vector machine," *Simul. Model. Pract. Theory*, vol. 18, no. 9, pp. 1412–1424, 2010.

[13] M. F. Guo and N. C. Yang, "Features-clustering-based earth fault detection using singular-value decomposition and fuzzy c-means in resonant grounding distribution systems," *Int. J. Electr. Power Energy Syst.*, vol. 93, pp. 97–108, Dec. 2017.

[14] H. Livani and C. Y. Evrenosoğlu, "A fault classification and localization method for three-terminal circuits using machine learning," *IEEE Trans. Power Del.*, vol. 28, no. 4, pp. 2282–2290, Oct. 2013.

[15] B. Y. Vyas, B. Das, and R. P. Maheshwari, "Improved fault classification in series compensated transmission line: Comparative evaluation of chebyshev neural network training algorithms," *IEEE Trans. Neural Netw. Learn. Syst.*, vol. 27, no. 8, pp. 1631–1642, Aug. 2016.

[16] M. Dehghani, M. H. Khooban, and T. Niknam, "Fast fault detection and classification based on a combination of wavelet singular entropy theory and fuzzy logic in distribution lines in the presence of distributed generations," *Int. J. Electr. Power Energy Syst.*, vol. 78, pp. 455–462, Jun. 2016.
[17] K. Chen, J. Hu, and J. He, "A framework for automatically extracting overvoltage features based on sparse autoencoder," *IEEE Trans. Smart Grid*, vol. 9, no. 2, pp. 594–604, Mar. 2018.
[18] S. B. Nagaraj, L. M. McClain, E. J. Boyle, D. W. Zhou, S. M. Ramaswamy, S. Biswal, O. Akeju, P. L. Purdon, and M. B. Westover, "Electroencephalogram based detection of deep sedation in ICU patients using atomic decomposition," *IEEE Trans. Biomed. Eng.*, vol. 65, no. 12, pp. 2684–2691, Dec. 2018.
[19] G. Szaszák, M. Á. Tündik, and B. Gerazov, "Prosodic stress detection for fixed stress languages using formal atom decomposition and a statistical hidden Markov hybrid," *Speech Commun.*, vol. 102, pp. 14–26, Sep. 2018.
[20] Q. Yang, J. Wang, W. Sima, L. Chen, and T. Yuan, "Mixed over-voltage decomposition using atomic decompositions based on a damped sinusoids atom dictionary," *Energies*, vol. 4, no. 9, pp. 1410–1427, Sep. 2011.
[21] S. G. Mallat and Z. Zhang, "Matching pursuits with time-frequency dictionaries," *IEEE Trans. Signal Process.*, vol. 41, no. 12, pp. 3397–3415, Dec. 1993.
[22] T. X. Zhu, "Detection and characterization of oscillatory transients using matching pursuits with a damped sinusoidal dictionary," *IEEE Trans. Power Del.*, vol. 22, no. 2, pp. 1093–1099, Apr. 2007.
[23] M. M. Hadji and B. Vahidi, "A solution to the unit commitment problem using imperialistic competition algorithm," *IEEE Trans. Power Syst.*, vol. 27, no. 1, pp. 117–124, Feb. 2012.
[24] M. F. Guo, X. D. Zeng, D. Y. Chen, and N. C. Yang, "Deep-learning-based earth fault detection using continuous wavelet transform and convolutional neural network in resonant grounding distribution systems," *IEEE Sensors J.*, vol. 18, no. 3, pp. 1291–1300, Feb. 2018.
[25] Q. Yang, H. Zhao, W. Sima, R. Han, and Y. Chen, "Identification method of grid measured over-voltage based on threshold judgment and support vector machine," *High Voltage Eng.*, vol. 42, no. 10, pp. 3188–3198, Oct. 2016.
[26] W. X. Sima, R. Ran, T. Yuan, A. M. Yao, L. Q. Ma, and D. K. Yang, "Identification of arc grounding over-voltage using mathematical morphology transform," *High Voltage Eng.*, vol. 36, no. 4, pp. 835–841, Apr. 2010.
[27] X. Li, Z. He, H. Huang, H. Ye, L. Wang, and L. Du, "Application research on over-voltage smart recognition system for 110kV substation," in *Proc. IEEE Int. Conf. High Voltage Eng. Appl.*, Chengdu, China, Sep. 2016, pp. 1–4.

WEI GAO was born in Pingtan, China, in 1983. He received the B.S. degree in electrical engineering and automation and the M.S. degrees in power system and automation from Fuzhou University, China, in 2005 and 2008, respectively. He is currently pursuing the Ph.D. degree with the National Taiwan University of Science and Technology, Taiwan. Since 2008, he has been a Lecturer with Fuzhou University. He has authored or coauthored about eight journal papers and one book, and holds about three patents. His research interests include generation technology of photovoltaic and faults diagnosis of power equipment.

RONG-JONG WAI (M'99–SM'05) was born in Tainan, Taiwan, in 1974. He received the B.S. degree in electrical engineering and the Ph.D. degree in electronic engineering from Chung Yuan Christian University, Chung Li, Taiwan, in 1996 and 1999, respectively. From 1998 to 2015, he was with Yuan Ze University, Chung Li, where he was the Dean of General Affairs, from 2008 to 2013, and the Chairman of the Department of Electrical Engineering, from 2014 to 2015. Since 2015, he has been with the National Taiwan University of Science and Technology, Taipei, Taiwan, where he is currently a Distinguished Professor, the Dean of General Affairs, and the Director of the Energy Technology and Mechatronics Laboratory. He has authored more than 170 conference papers, over 180 international journal papers, four book chapters, and 57 inventive patents. His research interests include power electronics, motor servo drives, mechatronics, energy technology, and control theory applications. The outstanding achievement of his research is for contributions to real-time intelligent control in practical applications and high-efficiency power converters in energy technology. He is a Fellow of the Institution of Engineering and Technology (U.K.) and a Senior Member of the Institute of Electrical and Electronics Engineers (USA).

YU-FEI LIAO was born in Longyan, China, in 1993. He received the B.S. degree from the Nanjing University of Science and Technology, Nanjing, China, in 2016, and the M.S. degree from Fuzhou University, Fuzhou, China, in 2019. He is currently with the Fuzhou Power Supply Company of State Grid Fujian Electric Power Company, China. His research interest includes faults diagnosis of power distribution systems.

MOU-FA GUO was born in Fuzhou, China, in 1973. He received the B.S. and M.S. degrees from Fuzhou University, Fuzhou, China, in 1996 and 1999, respectively, and the Ph.D. degree from Yuan Ze University, Taiwan, in 2018, all in electrical engineering. Since 2000, he has been with Fuzhou University, where he is currently a Professor, and the Chairman of the Department of Electric Power Engineering. His research interests include power distribution systems and its automation, application of artificial intelligence in power distribution systems.

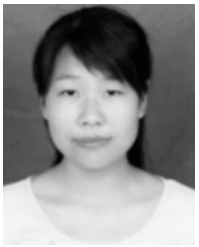

YAN YANG was born in Jiangsu, China, in 1984. She received the M.S. degrees from the China University of Mining and Technology, China, in 2009. She is currently pursuing the Ph.D. degree with the Department of Electrical Engineering and Computer Science, National Taiwan University of Science and Technology, Taipei, Taiwan. She is also a Lecturer with the Department of Automation, Huaiyin Institute of Technology, China. Her research interests include smart microgrids and non-linear control of power converter.